

WEIGHING GALAXY CLUSTERS WITH GAS. I. ON THE METHODS OF COMPUTING HYDROSTATIC MASS BIAS

ERWIN T. LAU^{1,2}, DAISUKE NAGAI^{1,2,3}, AND KAYLEA NELSON³

¹Department of Physics, Yale University, New Haven, CT 06520, USA; erwin.lau@yale.edu

²Yale Center for Astronomy and Astrophysics, Yale University, New Haven, CT 06520, USA

³Department of Astronomy, Yale University, New Haven, CT 06520, USA

The Astrophysical Journal, accepted

ABSTRACT

Mass estimates of galaxy clusters from X-ray and Sunyaev-Zel'dovich observations assume the intracluster gas is in hydrostatic equilibrium with their gravitational potential. However, since galaxy clusters are dynamically active objects whose dynamical states can deviate significantly from the equilibrium configuration, the departure from the hydrostatic equilibrium assumption is one of the largest sources of systematic uncertainties in cluster cosmology. In the literature there has been two methods for computing the hydrostatic mass bias based on the Euler and the modified Jeans equations, respectively, and there has been some confusion about the validity of these two methods. The word “Jeans” was a misnomer, which incorrectly implies that the gas is collisionless. To avoid further confusion, we instead refer these methods as “summation” and “averaging” methods respectively. In this work, we show that these two methods for computing the hydrostatic mass bias are equivalent by demonstrating that the equation used in the second method can be derived from taking spatial averages of the Euler equation. Specifically, we identify the correspondences of individual terms in these two methods mathematically and show that these correspondences are valid to within a few percent level using hydrodynamical simulations of galaxy cluster formation. In addition, we compute the mass bias associated with the acceleration of gas and show that its contribution is small in the virialized regions in the interior of galaxy clusters, but becomes non-negligible in the outskirts of massive galaxy clusters. We discuss future prospects of understanding and characterizing biases in the mass estimate of galaxy clusters using both hydrodynamical simulations and observations and their implications for cluster cosmology.

Subject headings: cosmology: theory – galaxies: clusters: general – methods: numerical – X-rays: galaxies: clusters

1. INTRODUCTION

Clusters of galaxies are the largest virialized objects in the Universe, promising to provide unique insights into both cosmology and astrophysics. Mass of galaxy clusters is one of the fundamental quantities for using clusters as cosmological and astrophysical probes. Cluster mass estimates from X-ray and Sunyaev-Zel'dovich (SZ) data assume the hydrostatic equilibrium (HSE) of gas in their gravitational potential. However, galaxy clusters are dynamical active objects, whose dynamical state deviates significantly from the equilibrium configuration. As a result, the hydrostatic mass bias is one of the largest sources of systematic uncertainties in cluster cosmology (Allen et al. 2008; Vikhlinin et al. 2009; Planck Collaboration XX 2013). To exploit the statistical power of the ongoing and upcoming multi-wavelength cluster surveys, the hydrostatic mass bias has to be understood and controlled at the level of a few percent.

To date, numerical simulations have been used extensively to characterize the hydrostatic mass bias and understand its origin. Hydrodynamical cluster simulations predict that the hydrostatic bias is at the level of 5% to 35%, depending on the dynamical state of clusters (e.g., Rasia et al. 2006; Nagai et al. 2007b; Jeltama et al. 2008; Piffaretti & Valdarnini 2008; Burns et al. 2010; Meneghetti et al. 2010). These simulations suggest that the bias is predominantly due to the effective non-thermal pressure support provided by bulk and turbulent gas flows induced by cluster mergers and accretion events (Lau et al. 2009; Vazza et al. 2009; Nelson et al. 2012). Comparison of weak lensing and X-ray hydrostatic mass further suggests that the hydrostatic mass bias at the level of $\lesssim 10\%$ for

the relaxed clusters and 15% to 20% for dynamically active systems (e.g., Zhang et al. 2010; Mahdavi et al. 2013).

In the literature, there are two methods for computing the bias. In the first method, the mass enclosed within a surface is determined by summing up contribution of each gas element on the surface its potential gradient, which is evaluated from the thermal pressure gradient and temporal and spatial gradients of gas velocities using the Euler equation (Fang et al. 2009; Suto et al. 2013). The second method, on the other hand, uses the potential gradient averaged over the surface, which is estimated from the averaged gas densities, pressure, and velocities using a modified version of the Jeans equation (Rasia et al. 2004; Lau et al. 2009; Nelson et al. 2012). There has been a question regarding the validity of the second method (Suto et al. 2013). This confusion has partly stemmed from the use of the word “Jeans”, a misnomer, which incorrectly implies that the gas is collisionless. To avoid further confusion, we refer them as the “summation” and “averaging” methods respectively hereafter.

Different authors have made a number of simplifying assumptions in computing the corrections terms in the hydrostatic mass bias with both methods. In Rasia et al. (2004) the mean and random components of the gas motions are not differentiated. In Fang et al. (2009) and Lau et al. (2009), the support due to rotational motions and streaming motions are explicitly included, but each arrived at a different conclusion about the relative importance of rotational versus random motions partly because of the different physical meanings of mass correction terms in the summation and averaging methods used respectively in those work. More recently Suto et al.

(2013) relaxed the steady state assumption of the cluster (i.e., $\partial \mathbf{v} / \partial t = 0$), and suggested that the acceleration of gas introduces extra bias whose magnitude is comparable to other mass bias terms.

The primary goal of this work is to assess the validity of two methods used to compute the hydrostatic mass bias and to understand its physical origin. In this work, we show that the summation and averaging methods for computing the hydrostatic mass bias are both valid by demonstrating that the averaging method can be derived from the summation method by applying spatial averaging over gas elements. This process introduces additional mean and dispersion terms in gas velocities that are absent in the original Euler equation. These extra terms originate from fluctuations in gas velocities that are implicitly included in the summation method, but must be explicitly accounted for in the averaging method. Using hydrodynamical simulations of cluster formation, we show that the correspondence between these two methods are robust at the level of a few percent. In addition, we compute the acceleration term directly using multiple time-steps of each simulated cluster and assess its relative importance. Finally, we argue that the averaging method is more suitable than the summation method for application to observational datasets.

This paper is organized as follows. In Section 2 we present the theoretical frameworks of cluster mass reconstruction using the summation and averaging methods. In Section 3, using numerical simulations we show the equivalence of the two methods and evaluate the importance of gas acceleration. In Section 4 we provide a summary and discuss implications of our results.

2. MASS RECONSTRUCTION: THEORY

2.1. Summation Method

Using Gauss's law for the gravitational field, the total gravitational mass enclosed within volume V with surface ∂V is

$$M = \frac{1}{4\pi G} \oint_{\partial V} \nabla \Phi \cdot d\mathbf{S}, \quad (1)$$

where M is the enclosed mass and Φ is the gravitational potential. The mass inside this surface is known when the potential gradient $\nabla \Phi$ is known at every position on the imaginary surface with differential surface element $d\mathbf{S}$.

The potential gradient is generally given by the dynamical evolution of any single particle component that constitutes the system. We start with the mass and momentum conservation equations in index notation:

$$\frac{\partial \rho}{\partial t} + \frac{\partial (\rho v^i)}{\partial x^i} = 0, \quad (2)$$

$$\frac{\partial (\rho v^i)}{\partial t} + \frac{\partial \tau^{ij}}{\partial x^j} = -\rho g^{ij} \frac{\partial \Phi}{\partial x^j}, \quad (3)$$

where ρ is the particle density, v^i is the i -th component of the particle velocity, and g^{ij} is the spatial metric tensor. Repeated indices are summed over. The momentum flux tensor (or stress tensor) is defined as

$$\tau^{ij} \equiv \overline{\rho v^i v^j} = \rho \sigma^{2,ij} + \rho u^i u^j, \quad (4)$$

where $u^i = \overline{v^i}$ and $\sigma^{2,ij} \equiv \overline{(v^i - u^i)(v^j - u^j)}$ is the velocity dispersion tensor. The overline denotes averaging over some volume of the system.

In the hydrodynamical limit where the mean free path of the gas particle is small compared to the scale of the system,

the gas particles undergo frequent collisions and their distribution is approximately Maxwellian. For such gas, viscosity is negligible and $\sigma^{2,ij}$ is isotropic with zero off-diagonal components. The momentum flux tensor is then given by

$$\tau^{ij} = \tau_E^{ij} \equiv P g^{ij} + \rho u^i u^j, \quad (5)$$

where P is the thermal pressure. The momentum conservation equation (Equation 3) then becomes the Euler equation when combined with the continuity equation (Equation 2):

$$\frac{\partial u^i}{\partial t} + u^j \frac{\partial u^i}{\partial x^j} = -\frac{1}{\rho} \frac{\partial P}{\partial x_i} - \frac{\partial \Phi}{\partial x_i}. \quad (6)$$

Using Gauss's Law (Equation 1), the mass is given by

$$M = \frac{-1}{4\pi G} \oint_{\partial V} \left(\frac{\partial u^i}{\partial t} + u^j \frac{\partial u^i}{\partial x^j} + \frac{1}{\rho} \frac{\partial P}{\partial x_i} \right) dS_i. \quad (7)$$

This mass can be broken down into various effective mass terms (Fang et al. 2009; Suto et al. 2013):

$$M(< r) = M_{\text{tot}}^S(< r) = M_{\text{therm}}^S + M_{\text{rot}}^S + M_{\text{stream}}^S + M_{\text{accel}}^S, \quad (8)$$

where the superscript S indicates that the mass terms are derived from applying the summation method. The individual terms in spherical coordinates (r, θ, ϕ) are

$$M_{\text{therm}}^S = \frac{-1}{4\pi G} \int \frac{1}{\rho} \frac{\partial P}{\partial r} r^2 d\Omega, \quad (9)$$

$$M_{\text{rot}}^S = \frac{1}{4\pi G} \int (u_\theta^2 + u_\phi^2) r d\Omega, \quad (10)$$

$$M_{\text{stream}}^S = \frac{-1}{4\pi G} \int \left(u_r \frac{\partial u_r}{\partial r} + \frac{u_\theta}{r} \frac{\partial u_r}{\partial \theta} + \frac{u_\phi}{r \sin \theta} \frac{\partial u_r}{\partial \phi} \right) r^2 d\Omega, \quad (11)$$

$$M_{\text{accel}}^S = \frac{-1}{4\pi G} \int \frac{\partial u_r}{\partial t} r^2 d\Omega, \quad (12)$$

where $d\Omega = \sin \theta d\theta d\phi$ is the solid angle element and we have adopted ∂V to be a spherical surface with radius r . The physical significance of the terms are as follows: M_{therm}^S is the term representing the support against gravity from the thermal pressure of the gas; M_{rot}^S is the sum of contribution of support due to tangential gas motions (which includes both mean and random motions); M_{stream}^S is the sum of support due to spatial variations of streaming gas motions in the radial direction; and M_{accel}^S is the sum of support due to temporal variations in the radial gas velocities, which is negative (positive) if there is net gas acceleration (deceleration) from the cluster center.

2.2. Averaging Method

In the hydrodynamical limit, each gas element follows the Euler equation (Equation 6). The momentum flux tensor for each *single* gas element is $\tau^{ij} = \tau_E^{ij}$, where u^i is the i -th component of the mean velocity of the gas element. Let $\langle \dots \rangle_w$ denote the averaging operator performed over some volume V containing a number of gas elements. The average value of any arbitrary quantity $f(\mathbf{x})$ is given by

$$\langle f \rangle_w(\mathbf{x}) = \int_V f(\mathbf{x} - \mathbf{x}') w(\mathbf{x}; \mathbf{x}') d^3 x', \quad (13)$$

where w is some normalized weight function $\int_V w d^3 x = 1$. When w is independent of \mathbf{x} , as in the case of volume averaging, $\langle f \rangle_w(\mathbf{x})$ is essentially the convolution $f * w$. The av-

eraging operator $\langle \dots \rangle_w$ then commutes with partial differentiation with respect to x , which follows from the convolution theorem: $\partial_x \langle f \rangle_w = \partial_x (f * w) = \partial_x f * w = \langle \partial_x f \rangle_w$. For density-weighted averaging, the weight function is the normalized density distribution, and the averaging operator can be expressed as $\langle \dots \rangle_\rho = \langle \rho \dots \rangle / \langle \rho \rangle$. Applying this volume averaging to the Euler momentum flux tensor τ_E^{ij} (Equation 5), we have

$$\begin{aligned} \langle \tau_E^{ij} \rangle &= \langle P g^{ij} \rangle + \langle \rho u^i u^j \rangle \\ &= \langle P g^{ij} \rangle + \langle \rho \rangle \langle u^i u^j \rangle_\rho \\ &= \langle P g^{ij} \rangle + \langle \rho \rangle \sigma_\rho^{2,ij} + \langle \rho \rangle \langle u^i \rangle_\rho \langle u^j \rangle_\rho, \end{aligned} \quad (14)$$

where $\langle u^i \rangle_\rho$ is the i -th component density-weighted average velocity of the gas elements in the considered volume V , and $\sigma_\rho^{2,ij} \equiv \langle (u^i - \langle u^i \rangle_\rho) (u^j - \langle u^j \rangle_\rho) \rangle_\rho$ is the density-weighted velocity dispersion tensor in the same volume V , which in general can be anisotropic and contain non-zero off-diagonal components.

Putting this averaged Euler momentum flux tensor (Equation 14) into the momentum conservation equation (Equation 3) and averaging other terms (e.g., $\rho u^i \rightarrow \langle \rho u^i \rangle = \langle \rho \rangle \langle u^i \rangle_\rho$) results in the following equation:

$$\begin{aligned} \frac{\partial \langle u^i \rangle_\rho}{\partial t} + \langle u^j \rangle_\rho \frac{\partial \langle u^i \rangle_\rho}{\partial x^j} + \frac{1}{\langle \rho \rangle} \frac{\partial \langle \rho \rangle \sigma_\rho^{2,ij}}{\partial x^i} \\ = - \frac{1}{\langle \rho \rangle} \frac{\partial \langle P \rangle}{\partial x_i} - \frac{1}{\langle \rho \rangle} \left\langle \rho \frac{\partial \Phi}{\partial x_i} \right\rangle. \end{aligned} \quad (15)$$

Here we have used the fact that the averaging operator $\langle \dots \rangle$ commutes with the partial differential operators ∂_t and ∂_x . Note that while this equation formally resembles the Jeans equation plus a thermal pressure gradient term, it does not imply that the gas is collisionless. This process of spatial averaging of the Euler equation is analogous to spatially filtering the Navier-Stokes equation that yields the Reynolds equation, in the presence of viscosity (e.g., Tennekes & Lumley 1972).

In spherical coordinates, the radial component of Equation (15) is given by

$$\begin{aligned} \frac{\partial \langle u_r \rangle_\rho}{\partial t} + \langle u_r \rangle_\rho \frac{\partial \langle u_r \rangle_\rho}{\partial r} + \frac{\langle u_\theta \rangle_\rho}{r} \frac{\partial \langle u_r \rangle_\rho}{\partial \theta} + \frac{\langle u_\phi \rangle_\rho}{r \sin \theta} \frac{\partial \langle u_r \rangle_\rho}{\partial \phi} \\ + \frac{1}{\langle \rho \rangle} \left(\frac{\partial \langle \rho \rangle \sigma_{\rho,rr}^2}{\partial r} + \frac{1}{r} \frac{\partial \langle \rho \rangle \sigma_{\rho,r\theta}^2}{\partial \theta} + \frac{1}{r \sin \theta} \frac{\partial \langle \rho \rangle \sigma_{\rho,r\phi}^2}{\partial \phi} \right) \\ + \frac{1}{r} (2\sigma_{\rho,rr}^2 - \sigma_{\rho,\theta\theta}^2 - \sigma_{\rho,\phi\phi}^2 - \langle u_\theta \rangle_\rho^2 - \langle u_\phi \rangle_\rho^2 + \sigma_{\rho,r\theta}^2 \cot \theta) \\ = - \frac{1}{\langle \rho \rangle} \frac{\partial \langle P \rangle}{\partial r} - \frac{1}{\langle \rho \rangle} \left\langle \rho \frac{\partial \Phi}{\partial r} \right\rangle. \end{aligned} \quad (16)$$

Assuming spherical symmetry and averaging over the surface of the imaginary sphere with radius r , the last term in this equation can be expressed in terms of the mass enclosed within r :

$$\frac{1}{\langle \rho \rangle} \left\langle \rho \frac{\partial \Phi}{\partial r} \right\rangle = \frac{1}{\langle \rho \rangle} \left\langle \rho \frac{GM(< r)}{r^2} \right\rangle = \frac{GM(< r)}{r^2} \quad (17)$$

where we have used the fact that mass is unchanged by averaging. As with the summation method, the total mass enclosed within radius r can also be broken down into different

effective mass terms:

$$\begin{aligned} M(< r) = M_{\text{tot}}^A(< r) = M_{\text{therm}}^A + M_{\text{rand}}^A + M_{\text{rot}}^A \\ + M_{\text{cross}}^A + M_{\text{stream}}^A + M_{\text{accel}}^A, \end{aligned} \quad (18)$$

with

$$M_{\text{therm}}^A = \frac{-r^2}{G \langle \rho \rangle} \frac{\partial \langle P \rangle}{\partial r}, \quad (19)$$

$$M_{\text{rand}}^A = \frac{-r^2}{G \langle \rho \rangle} \frac{\partial \langle \rho \rangle \sigma_{\rho,rr}^2}{\partial r} - \frac{r}{G} (2\sigma_{\rho,rr}^2 - \sigma_{\rho,\theta\theta}^2 - \sigma_{\rho,\phi\phi}^2), \quad (20)$$

$$M_{\text{rot}}^A = \frac{r}{G} (\langle u_\theta \rangle_\rho^2 + \langle u_\phi \rangle_\rho^2), \quad (21)$$

$$M_{\text{stream}}^A = \frac{-r^2}{G} \left(\langle u_r \rangle_\rho \frac{\partial \langle u_r \rangle_\rho}{\partial r} + \frac{\langle u_\theta \rangle_\rho}{r} \frac{\partial \langle u_r \rangle_\rho}{\partial \theta} + \frac{\langle u_\phi \rangle_\rho}{r \sin \theta} \frac{\partial \langle u_r \rangle_\rho}{\partial \phi} \right), \quad (22)$$

$$\begin{aligned} M_{\text{cross}}^A = \frac{-r^2}{G \langle \rho \rangle} \left(\frac{1}{r} \frac{\partial \langle \rho \rangle \sigma_{\rho,r\theta}^2}{\partial \theta} + \frac{1}{r \sin \theta} \frac{\partial \langle \rho \rangle \sigma_{\rho,r\phi}^2}{\partial \phi} \right) \\ - \frac{r}{G} (\sigma_{\rho,r\theta}^2 \cot \theta), \end{aligned} \quad (23)$$

$$M_{\text{accel}}^A = \frac{-r^2}{G} \frac{\partial \langle u_r \rangle_\rho}{\partial t}, \quad (24)$$

where the superscript A denotes that the mass terms are derived from the averaging method (Equation 15). Except for M_{accel}^A , all of the above mass terms are the same as Equations (7) – (11) in Lau et al. (2009) where the gas density and pressure are volume averaged and the velocities are density-weighted averaged over the spherical surface. The physical significance of the terms are as follows: M_{therm}^A is the term representing the support against gravity from the averaged thermal pressure of the gas; M_{rand}^A is the support from the random motions of gas in both the radial and tangential directions; M_{rot}^A is the rotational support due to *mean* tangential motions of gas; M_{stream}^A comes from spatial variations of the *mean* radial streaming gas velocities; M_{cross}^A arises from the off-diagonal components of the velocity dispersion tensor, which are non-zero if the radial and tangential components of the random motions are correlated; and M_{accel}^A is the support due to temporal variations of the *mean* radial gas velocities at a fixed radius, which is negative (positive) for net gas accelerating (decelerating) away from the cluster center.

2.3. Correspondence between the Summation and Averaging Methods

Both M_{tot}^S and M_{tot}^A are estimates of the total mass using gas properties. They are both derived from the Euler equations with the application of Gauss's Law, but there are notable differences in how gas properties are handled. In the summation method, gas properties are summed over the surface containing the enclosed mass. In the averaging method, the quantities are averaged over the spherical surface. Specifically, each mass term in M_{tot}^S has corresponding term in M_{tot}^A ,

$$M_{\text{therm}}^S \Leftrightarrow M_{\text{therm}}^A, \quad (25)$$

$$M_{\text{stream}}^S \Leftrightarrow M_{\text{rand}}^A + M_{\text{stream}}^A + M_{\text{cross}}^A, \quad (26)$$

$$M_{\text{rot}}^S \Leftrightarrow M_{\text{rot}}^A, \quad (27)$$

$$M_{\text{accel}}^S \Leftrightarrow M_{\text{accel}}^A, \quad (28)$$

where

$$M_{\text{rand}}^{A'} = M_{\text{rand}}^A - \frac{r}{G} (\sigma_{\rho, \theta\theta}^2 + \sigma_{\rho, \phi\phi}^2), \quad (29)$$

$$M_{\text{rot}}^{A'} = M_{\text{rot}}^A + \frac{r}{G} (\sigma_{\rho, \theta\theta}^2 + \sigma_{\rho, \phi\phi}^2). \quad (30)$$

Note that the rotation term in the summation method is different from the one in the averaging method: M_{rot}^S includes both the *mean* and *random* parts of the tangential components, while M_{rot}^A only accounts for the *mean* tangential motions. When comparing the rotational term between the two methods, one should use $M_{\text{rot}}^{A'}$ which includes both the *mean* and *random* parts of the tangential components. Likewise for the streaming term, M_{stream}^S should be compared to $M_{\text{stream}}^{A'}$ instead of M_{stream}^A . In the following section, we use numerical simulations to demonstrate the equivalence of the two methods by evaluating individual terms in M_{tot}^S and M_{tot}^A .

3. MASS RECONSTRUCTION: SIMULATION

3.1. Data

In this work, we use high resolution cosmological hydrodynamical simulations presented in Nagai et al. (2007a,b); Lau et al. (2009); Nelson et al. (2012). Here we provide a brief description of the simulations, and we refer the readers to Nagai et al. (2007a,b) for details. The simulations are based on the flat concordance Λ CDM model: $\Omega_m = 1 - \Omega_\Lambda = 0.3$, $\Omega_b = 0.04286$, $h = 0.7$ and $\sigma_8 = 0.9$, where the Hubble constant is defined as $100h \text{ km s}^{-1} \text{ Mpc}^{-1}$, and σ_8 is the power spectrum normalization on an $8h^{-1} \text{ Mpc}$ scale. They were performed with the Adaptive Refinement Tree (ART) N -body+gasdynamics code (Kravtsov 1999; Kravtsov et al. 2002; Rudd et al. 2008), an Eulerian code that uses adaptive refinement in space and time, and (non-adaptive) refinement in mass (Klypin et al. 2001) to reach the high dynamic range required to resolve cores of halos formed in self-consistent cosmological simulations. They were run using a uniform 128^3 grid and 8 levels of mesh refinement in computational boxes of $120h^{-1} \text{ Mpc}$ and $80h^{-1} \text{ Mpc}$ on a side with peak resolution of $\approx 3.66h^{-1} \text{ kpc}$ and $2.44h^{-1} \text{ kpc}$ respectively. The dark matter (DM) particle mass in the regions around each cluster was $9.1 \times 10^8 h^{-1} M_\odot$ and $2.7 \times 10^8 h^{-1} M_\odot$ for the two box sizes, while other regions were simulated with lower mass resolution.

For this paper, we analyzed five most relaxed clusters at $z = 0.026$ in the sample, re-simulated with non-radiative gas physics used in both Lau et al. (2009) and Nelson et al. (2012). We selected relaxed clusters to focus on a clean sample ideal for testing the two methods in question. We examine the dependence of hydrostatic mass bias on cluster dynamical states in our second paper (Nelson et al. 2013). Table 1 gives their r_{500c} , which is the radius enclosing an average total mass density of 500 times the critical density of the universe, and the corresponding enclosed mass M_{500c} . As shown in Lau et al. (2009), radiative cooling, star formation and supernova feedback have little effect on the hydrostatic mass bias and total mass recovery from gas motions, although the relative contributions of different mass terms do change near the cluster core.

3.2. Method

To compute each mass term in both the summation and averaging methods presented in Section 2, we work in the

TABLE 1
PROPERTIES OF THE SIMULATED CLUSTERS

Cluster ID	M_{500c} [$10^{14} h^{-1} M_\odot$]	r_{500c} [$h^{-1} \text{ Mpc}$]	Box size [$h^{-1} \text{ Mpc}$]
CL104	5.19	0.956	120
CL3	2.09	0.706	80
CL7	1.18	0.584	80
CL10	0.62	0.471	80
CL14	0.64	0.576	80

spherical coordinate system (r, θ, ϕ) , and divide the analysis region into 80 spherical logarithmic bins from $10h^{-1} \text{ kpc}$ to $10h^{-1} \text{ Mpc}$ in the radial direction from the cluster center, defined as the position with the maximum binding energy. Each spherical bin is further subdivided into 60 and 120 uniform angular bins in the θ and ϕ directions, respectively. Our results are insensitive to the exact choice of binning. We choose the rest frame of the system to be the center-of-mass velocity of the total mass interior to each radial bin. This is different from Lau et al. (2009) where the rest frame of the system is defined to be the mass-weighted average DM velocity interior to r_{500c} , but the results presented here are insensitive to the choice of the rest frame. We rotate the coordinate system for each radial bin such that the z -axis aligns with the axis of the total gas angular momentum of that bin.

For M_{tot}^S , we compute gas velocities, density and pressure in each angular bin by taking average values (with appropriate weighting) of each quantity for the hydro cells residing in the angular bin. The derivatives of velocity and pressure are computed directly by differencing the neighboring angular bins. We then sum the relevant terms times the surface area $r^2 \Delta \cos \theta \Delta \phi$ for each angular bin over the spherical surface $4\pi r^2$ as in Equations (9) – (11). For M_{tot}^A , we compute each term in Equations (19) – (22) by averaging values of the angular bins over the radial bin. The acceleration term $M_{\text{accel}}^S = M_{\text{accel}}^A$ is computed explicitly by taking the difference of the radial velocity at the same radial bin between two consecutive time-steps divided by the time between these two snapshots. One cluster in our sample (CL104) has fine time resolution of $\sim 0.04 \text{ Gyr}$, while the other clusters have coarser time resolution of $\sim 0.35 \text{ Gyr}$. We have checked that the acceleration term is insensitive to the choice of time resolution within this range. We remove large gas substructures that may bias the global gas pressure and velocity gradients by applying the clump exclusion method presented in Zhuravleva et al. (2013). In addition, we smooth each mass term by applying the Savitzky-Golay filter used in Lau et al. (2009). Finally, the true mass M_{true} is directly computed from the simulations.

3.3. Results

Figure 1 shows the comparison between the true mass M_{true} , hydrostatic mass M_{therm}^S and M_{therm}^A , and the recovered masses M_{tot}^S and M_{tot}^A , together with their deviations from the true mass as a function of normalized cluster centric radius, r/r_{500c} . We note the the hydrostatic mass for both methods are essentially identical $M_{\text{therm}} = M_{\text{therm}}^S = M_{\text{therm}}^A$. On average, the recovery of the true mass profile is accurate at the level of a few percent at $r \approx r_{500c}$ for both summation and averaging methods. The acceleration term makes small contribution at $r \lesssim r_{500c}$, but its contribution becomes non-negligible at $r > r_{500c}$. For $r > r_{500c}$, M_{tot}^S and M_{tot}^A overestimates the true mass by $\sim 5\%$, mainly due to the acceleration term M_{accel} .

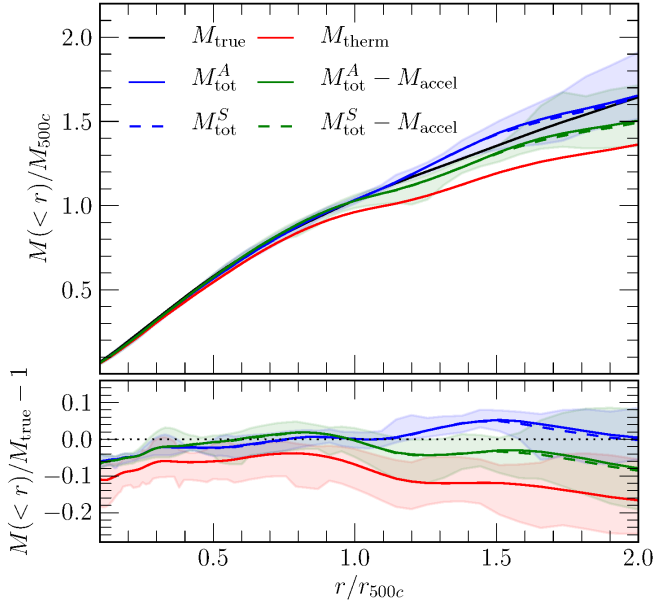


FIG. 1.— *Upper panel*: comparison between the true mass M_{true} (black line), the hydrostatic mass M_{therm} (red line) and total recovered masses M_{tot}^S (dashed lines) and M_{tot}^A (solid lines) with acceleration terms (blue lines) and without (green lines). The profiles are averaged over the cluster sample, with mass and radius normalized to M_{500c} and r_{500c} . The shaded regions show $\pm 1\sigma$ scatter. *Lower panel*: comparison between the deviation from the true mass M_{true} for the hydrostatic mass M_{therm} (red line) and recovered mass M^S (dashed lines) and M^A (solid lines) with acceleration terms (blue lines) and without (green lines). The shaded regions show $\pm 1\sigma$ scatter for the terms in the averaging method (solid lines).

Ignoring this term leads to a slight underestimate of the true mass.

Figure 2 shows the comparison of different mass terms in M^S and M^A in units of the true mass. For the averaging method, the random motion M_{rand}^A is a dominant term, contributing to $\sim 5\%$ of the mass support at $r = r_{500c}$, followed by the rotational term M_{rot}^A , the acceleration term M_{accel} , and the streaming term M_{stream}^A . The crossing term M_{cross}^A is very small ($\sim 0.01\%$), suggesting that the correlation among different velocity components is close to zero. At $r \gtrsim r_{500c}$, while the random motion term M_{rand}^A increases with radius, the acceleration term becomes comparable to M_{rand}^A , but with large fluctuations. The streaming term M_{stream}^A is small compared to M_{rand}^A . This term and the crossing term M_{cross}^A are ignored in Nelson et al. (2012) as they are negligibly small. However for individual clusters the streaming term can become comparable to the random motion term. For the Euler’s case, the dominant term at all radii is the M_{rot}^S , which represents the sum of support from tangential motions from all gas elements. The acceleration term again can be comparable to M_{rot}^S , although with large scatter. The streaming term M_{stream}^S is small but non-negligible.

Figure 2 also shows the comparison of the rotational and streaming terms for the summation and averaging methods: $M_{\text{rot}}^{A'}$ and $M_{\text{stream}}^{A'}$. In Section 2.3 we showed that the two are mathematically identical, and it is indeed the case for our simulated clusters: i.e., the terms in these two methods agree to better than a few percent for the relaxed clusters. Note that

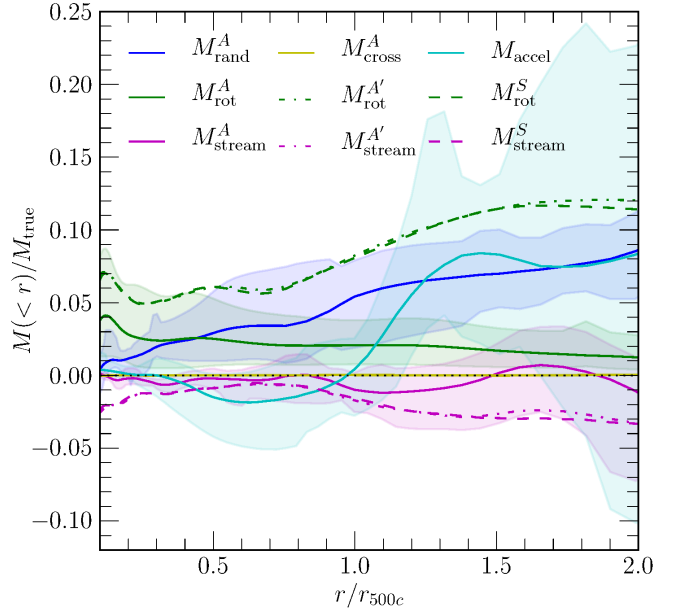


FIG. 2.— Comparison between the different mass terms divided by the true mass in the mass estimates based on the summation method: M_{rot}^A (green dashed), M_{stream}^A (magenta dashed); and the averaging method M_{rand}^A (blue solid), M_{rot}^A (green solid), M_{stream}^A (magenta solid), M_{cross}^A (yellow solid). The dot-dashed lines are $M_{\text{rot}}^{A'}$ (green) and $M_{\text{stream}}^{A'}$, which correspond to M_{rot}^S and M_{stream}^S . The profiles are averaged over the cluster sample, with mass and radius normalized to M_{500c} and r_{500c} . The shaded regions show $\pm 1\sigma$ scatter for the terms in the averaging method (solid lines).

$M_{\text{rot}}^S \simeq M_{\text{rot}}^{A'} > M_{\text{rot}}^A$ because both M_{rot}^S and $M_{\text{rot}}^{A'}$ account for the *mean* and *random* components of the tangential motions, while M_{rot}^A only accounts for the mean component. This partly explains the difference in the contribution from rotational support between Fang et al. (2009) and Lau et al. (2009) who computed M_{rot}^S and M_{rot}^A , respectively, despite the fact that they analyzed the same set of simulated clusters.

Our averaged M_{tot}^S agree qualitatively with the results of Suto et al. (2013). The acceleration terms M_{accel} in their work and ours become large in the cluster outskirts. Their streaming term M_{stream}^S is slightly larger in magnitude, but still consistent within $\sim 2\sigma$ scatter of our results. Their rotational term M_{rot}^S is also slightly larger than ours, mainly because their simulated cluster includes effects of radiative cooling and star formation that lead to “overcooling”, thereby increasing the rotational motion in the cluster core (Fang et al. 2009; Lau et al. 2011). This effect is also sensitive to the actual implementation of gas physics and the dynamical state of the cluster.

4. SUMMARY AND DISCUSSION

In this work, we show that two methods of computing the hydrostatic mass bias based on summation and averaging are equally valid and in fact equivalent. In the first method, contributions from individual gas element are summed over the imaginary surface one by one. The second method, on the other hand, uses gas velocities averaged over the surface. We show that the averaging method can be derived from the summation method by spatially averaging the terms in Euler equation. Specifically, we identify the correspondences of individual terms in these two methods mathematically and show that they are indeed valid to within few percent using hydrody-

namical simulations of galaxy cluster formation. In addition, we compute mass bias corrections associated with gas acceleration, which is generally small in the interior virialized regions of galaxy clusters, but becomes non-negligible in the outskirts of massive clusters where materials are still actively accreting today.

In observations we generally do not have access to small-scale properties of the intracluster medium below the instrumental resolution limits. Therefore the averaging method is more suitable for analyzing observational datasets because it is based on spatially-averaged quantities that can be derived directly from observations with finite spatial resolution. For example, the mean gas velocity and gas velocity dispersion averaged over some range of spatial scales in the averaging method can be measured with the upcoming ASTRO-H mission¹ via Doppler shift and broadening of heavy ion lines. Observationally, it is also difficult to measure gas acceleration, which introduces an irreducible bias. Simulations of cluster formation may be helpful in calibrating the gas acceleration term associated with the change in gas accretion rate and/or gas velocity profiles.

There are additional limitations for both methods when analyzing real clusters. In this work, we have assumed that the cluster gas is inviscid and unmagnetized and its mean free path is much smaller than the spatial resolution of the simulations. However, the mean free path of the gas in the cluster outskirts can become large such that the hydrodynamic approximation breaks down. In real clusters where the intracluster medium is likely to have tangled magnetic fields (as the magnetic energy density is considerably smaller than the thermal energy density), electron-ion pairs in the intracluster plasma perform random walk, giving rise to a finite effective mean free path, which might be a finite fraction of the Spitzer's value. Finite mean free path also gives a rise to non-zero physical viscosity and transport coefficients, whose

exact values are still unknown. A non-zero viscous stress tensor can then introduce additional support against gravity, and it must be included in the momentum flux tensor in both summing and averaging methods. Magnetic field and cosmic rays further give rise to additional mass correction terms associated with magnetic and cosmic ray pressure as well as their advection terms at the level of few percent. Even when the magnetic field is dynamically unimportant, magnetothermal instability may amplify turbulent motions, which could provide additional 5% to 30% of non-thermal pressure support (Parrish et al. 2012). All these effects can change the relative contributions of different types of gas motions to the effective mass correction terms.

In this work, we focused on a small number of relaxed clusters in order to test two methods in questions. However, mass biases are expected to be larger for unrelaxed clusters. It is therefore important to characterize the distribution of hydrostatic mass biases for a wide range of masses, redshifts, dynamical states, and accretion histories by analyzing a large cosmologically representative sample of galaxy clusters. In our second paper (Nelson et al. 2013), we use a large statistical mass-limited sample of simulated galaxy clusters to investigate these issues. Such work might also help better assess the current tension between Planck primary CMB and SZ cluster counts results (Planck Collaboration XX 2013).

We thank Andrea Morandi, Elena Rasia, Suto et al., and the anonymous referee for useful comments on the manuscript. This work was supported in part by NSF grant AST-1009811, NASA ATP grant NNX11AE07G, NASA Chandra Theory grant GO213004B, the Research Corporation, and by the facilities and staff of the Yale University Faculty of Arts and Sciences High Performance Computing Center.

REFERENCES

- Allen, S. W., Rapetti, D. A., Schmidt, R. W., et al. 2008, *MNRAS*, 383, 879
 Burns, J. O., Skillman, S. W., & O'Shea, B. W. 2010, *ApJ*, 721, 1105
 Fang, T., Humphrey, P., & Buote, D. 2009, *ApJ*, 691, 1648
 Jeltema, T. E., Hallman, E. J., Burns, J. O., & Motl, P. M. 2008, *ApJ*, 681, 167
 Klypin, A., Kravtsov, A. V., Bullock, J. S., & Primack, J. R. 2001, *ApJ*, 554, 903
 Kravtsov, A. V. 1999, PhD thesis, New Mexico State Univ.
 Kravtsov, A. V., Klypin, A., & Hoffman, Y. 2002, *ApJ*, 571, 563
 Lau, E. T., Kravtsov, A. V., & Nagai, D. 2009, *ApJ*, 705, 1129
 Lau, E. T., Nagai, D., Kravtsov, A. V., & Zentner, A. R. 2011, *ApJ*, 734, 93
 Mahdavi, A., Hoekstra, H., Babul, A., et al. 2013, *ApJ*, 767, 116
 Meneghetti, M., Rasia, E., Merten, J., et al. 2010, *A&A*, 514, A93
 Nagai, D., Kravtsov, A. V., & Vikhlinin, A. 2007a, *ApJ*, 668, 1
 Nagai, D., Vikhlinin, A., & Kravtsov, A. V. 2007b, *ApJ*, 655, 98
 Nelson, K., Lau, E. T., Nagai, D., Rudd, D. H., & Yu, L. 2013, *ApJ*, submitted, arXiv:1308.6589
 Nelson, K., Rudd, D. H., Shaw, L., & Nagai, D. 2012, *ApJ*, 751, 121
 Parrish, I. J., McCourt, M., Quataert, E., & Sharma, P. 2012, *MNRAS*, 419, L29
 Piffaretti, R., & Valdarnini, R. 2008, *A&A*, 491, 71
 Planck Collaboration XX. 2013, *A&A*, submitted, arXiv:1303.5080
 Rasia, E., Tormen, G., & Moscardini, L. 2004, *MNRAS*, 351, 237
 Rasia, E., Ettori, S., Moscardini, L., et al. 2006, *MNRAS*, 369, 2013
 Rudd, D. H., Zentner, A. R., & Kravtsov, A. V. 2008, *ApJ*, 672, 19
 Suto, D., Kawahara, H., Kitayama, T., et al. 2013, *ApJ*, 767, 79
 Tennekes, H., & Lumley, J. L. 1972, *A First Course in Turbulence* (Cambridge, MA, USA: MIT Press)
 Vazza, F., Brunetti, G., Kritsuk, A., et al. 2009, *A&A*, 504, 33
 Vikhlinin, A., Kravtsov, A. V., Burenin, R. A., et al. 2009, *ApJ*, 692, 1060
 Zhang, Y.-Y., Okabe, N., Finoguenov, A., et al. 2010, *ApJ*, 711, 1033
 Zhuravleva, I., Churazov, E., Kravtsov, A., et al. 2013, *MNRAS*, 428, 3274

¹ <http://astro-h.isas.jaxa.jp/>